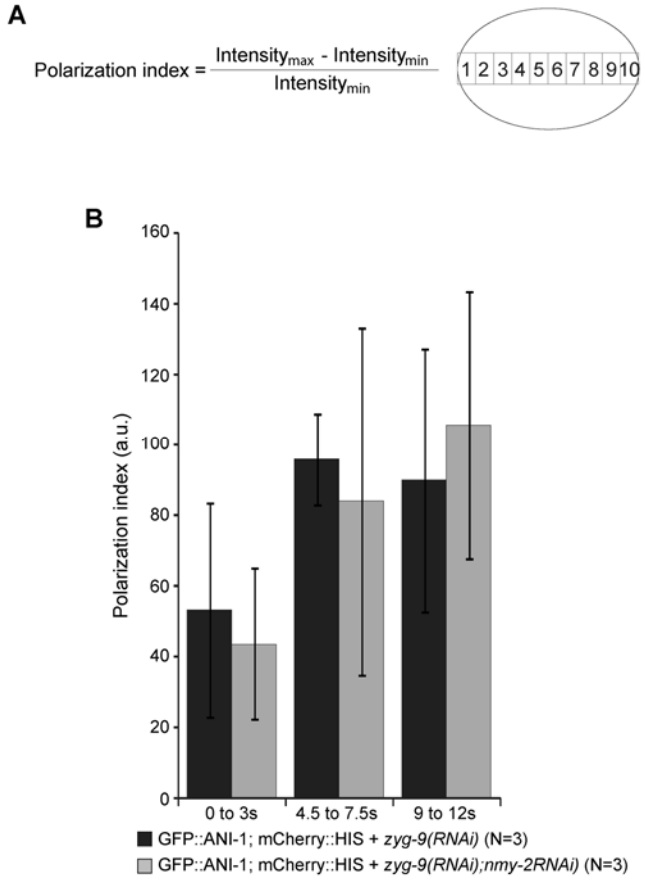

Figure S1

Myosin depletion does not significantly alter anillin polarization in embryos with posterior spindles. (A) Schematic and equation used to calculate the polarization index. (B) Quantification of extent of polarized recruitment of GFP::ANI-1 in embryos depleted of ZYG-9 alone or depleted of both ZYG-9 and NMY-2. Error bars represent ± SEM.

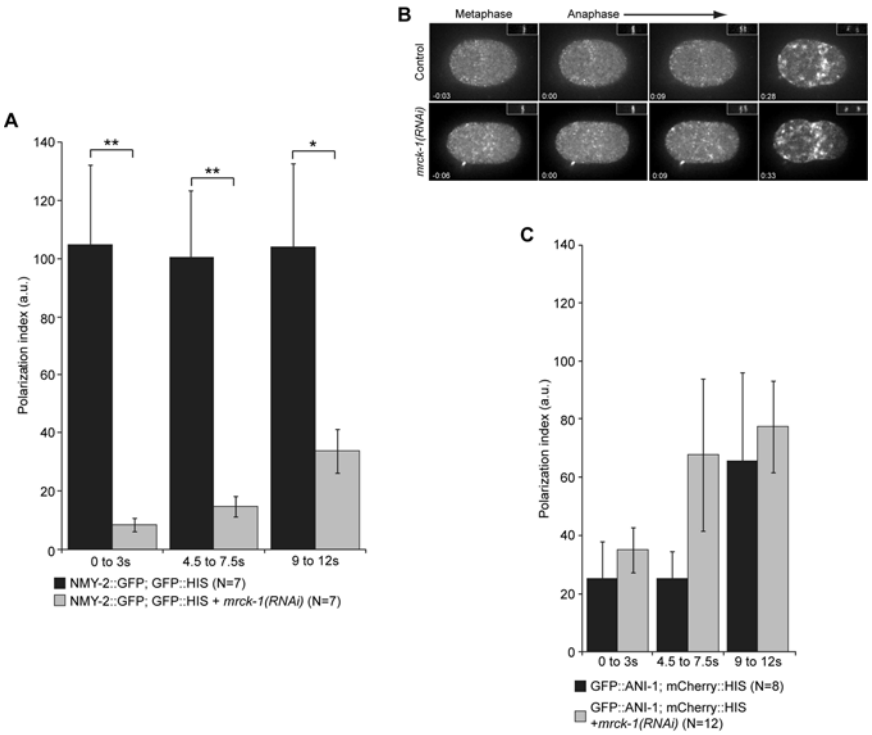

Figure S2

MRCK-1 depletion blocks the formation of the polarity cap of NMY-2::GFP and does not significantly alter anillin recruitment during anaphase. (A) Quantification of the GFP intensity in NMY-2::GFP control embryos and MRCK-1-depleted embryos. (B) The distribution of cortical GFP::ANI-1 in control and MRCK-1 depleted embryos are shown during metaphase and anaphase. Cell cycle timing was determined by mCherry::HIS (insets, top right). All images are projections of 5 planes spanning 2 μm. (C) Quantification of the degree of polarization of GFP::ANI-1 in control embryos and MRCK-1-depleted embryos. Error bars represent ± SEM; Single asterisk represents $p<0.05$; double asterisk represents $p<0.01$ from paired t-tests. 10 ⌈m scale bar.

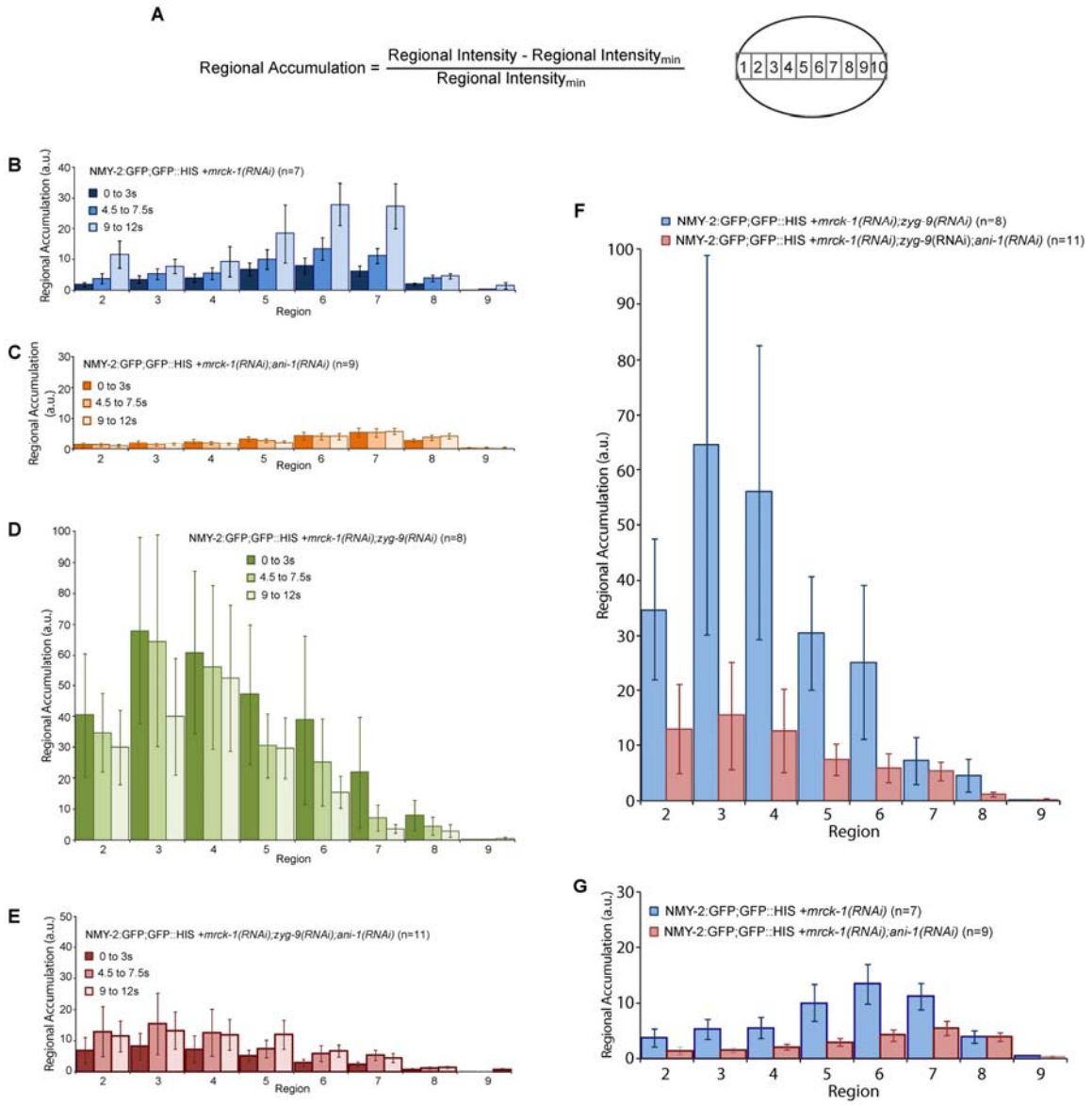

Figure S3

Anillin promotes the polarized accumulation of myosin. (A) Schematic and equation used to calculate normalized myosin intensity profiles. (B-E) The distribution of cortical NMY-2::GFP are quantified in embryos depleted of MRCK-1 (B), MRCK-1 and ANI-1 (C), MRCK-1 and ZYG-9 (D) and MRCK-1, ZYG-9 and ANI-1 (E). In ANI-1-depleted embryos, there is only slightly more NMY-2::GFP recruitment in the equatorial region (region 6 and 7) and anterior pole (region 2) as compared to the remaining regions. In addition, the intensity gradient along the AP axis is greatly reduced in *mrck-1(RNAi);zyg-9(RNAi);ani-1(RNAi)* embryos as compared to *mrck-1(RNAi);zyg-9(RNAi)* embryos. (F-G) The distribution of NMY-2::GFP from 4.5 s to 7.5 s after anaphase onset calculated as in (B-E).

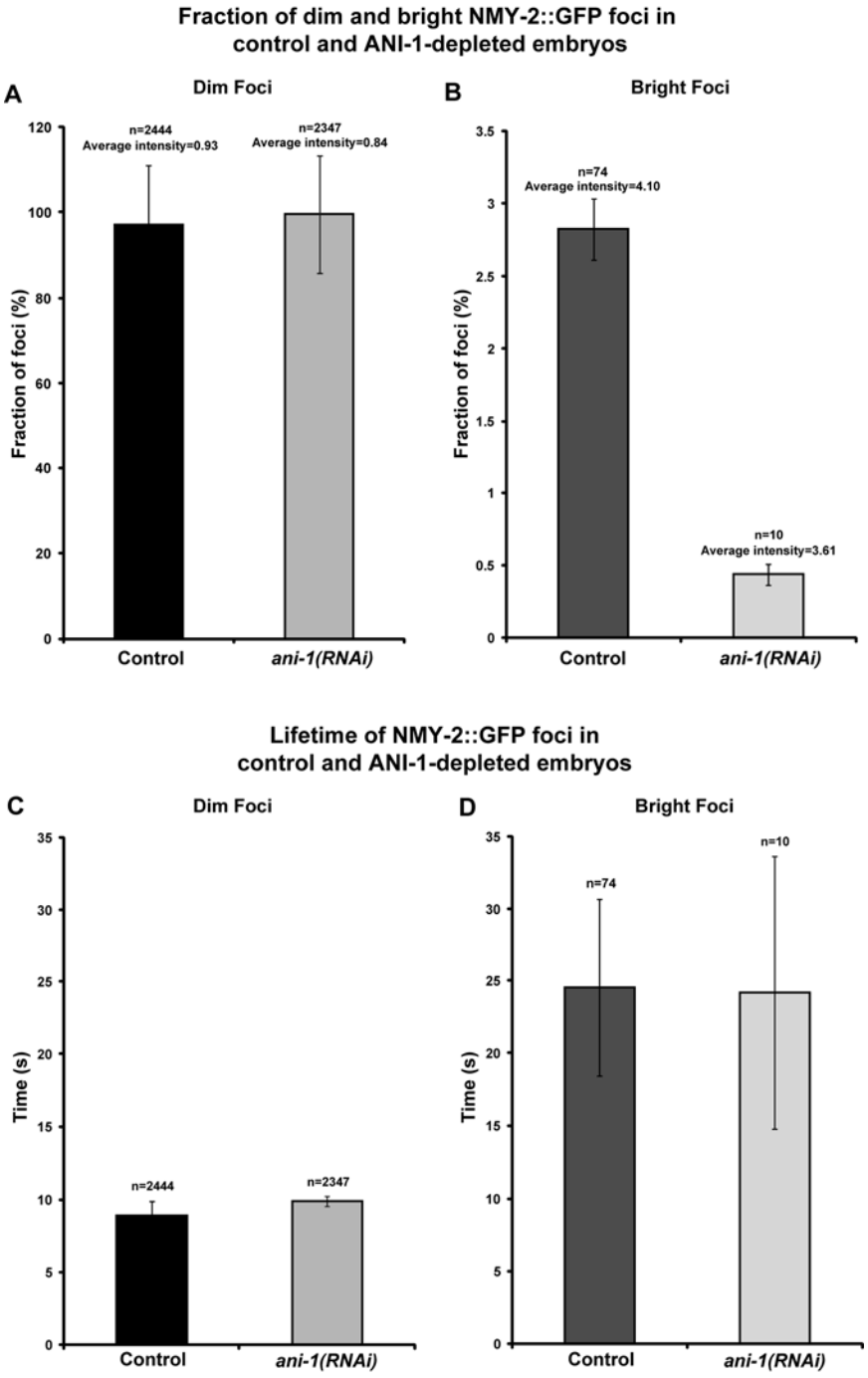

Figure S4

Depletion of anillin reduces the fraction of bright NMY-2::GFP foci. Fraction of dim (A) and bright (B) NMY-2::GFP foci in control and *ani-1(RNAi)* embryos. The percentage of foci with bright GFP signals is significantly reduced in ANI-1-depleted embryos. (C and D) Lifetime of NMY-2::GFP foci in control embryos (C) and *ani-1(RNAi)* embryos (D). No significant difference on the lifetime of bright and dim NMY-2::GFP foci in control and ANI-1-depleted embryos.

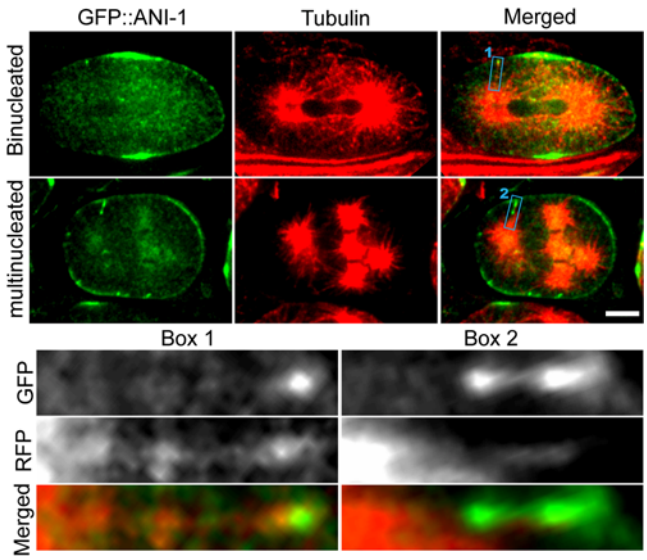

Figure S5

Anillin associates with microtubules. Embryos expressing GFP::ANI-1 were fixed and immunostained to detect endogenous tubulin (red) and GFP::ANI-1 (green). The boxed regions are shown at higher magnification below.

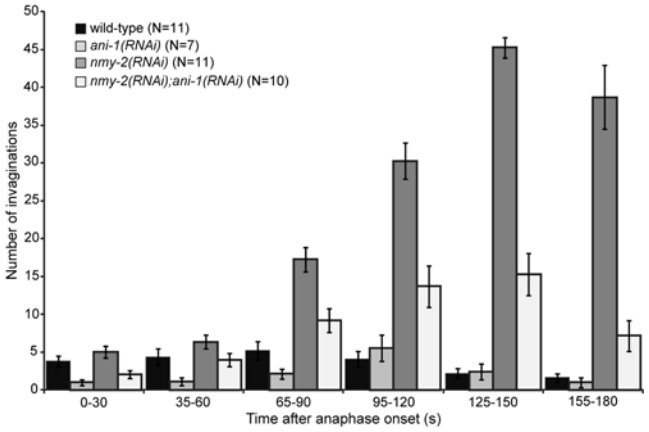

Figure S6

Quantitative analysis of the appearance of cortical invaginations. At 30 s intervals after anaphase onset (t=0) in embryos of the indicated genotypes expressing GFP::PH; mCherry::HIS were quantified as described in materials and methods. Error bars are ±SEM.

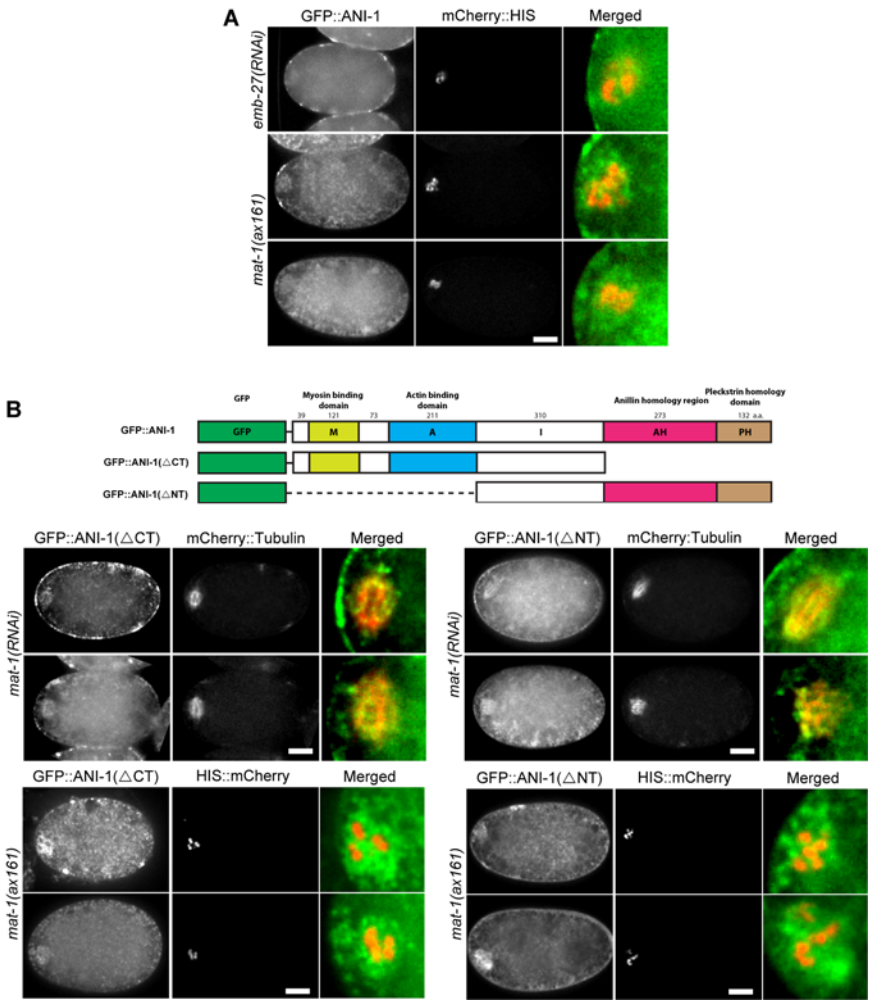

Figure S7

Anillin concentrates on meiotic spindles. (A) GFP::ANI-1 distribution in APC/C defective fertilized oocytes (due to depletion of EMB-27 by RNAi or the *mat-1(ax161)* mutation). (B) The distribution of GFP::ANI-1(ΔCT) and GFP::ANI-1(ΔNT) in meiotically-arrested fertilized oocytes.

Table S1. *C. elegans* strains used in this study.

Strain #	Marker	Genotype
N2	-	Ancestral N2 Bristol strain; “wild-type”
DH244	-	*zyg-9(b244)II*
DS77	-	*mat-1(ax161) I; him-8(e1489) IV*
AZ212	GFP::HIS	*unc-119(ed3) III ruIs32 [pAZ132: pie-1::GFP::histoneH2B] III.*
AZ244	GFP::Tubulin	*ruIs57[pie-1::GFP::tubulin + unc-119(+)]*
JA1559	mCherry::Tubulin	*unc-119(ed3) III; [mCherry::Tubulin]*
JH1327	PIE-1::GFP	*axEx73[pie-1::PIE-1::GFP]*
JJ1473	NMY-2::GFP	*unc-119(ed3) III; zuIs45 [nmy-2::NMY-2::GFP + unc-119(+)] V.*
KK866	GFP::PAR-2	*itIs153 [pie-1::PAR-2::GFP]*
OD38	GFP::ANI-1	*unc-119(ed3) III; ltIs28 [pASM14; pie-1::GFP-TEV-STag::ani-1; unc-119 (+)]*
OD58	GFP::PH	*unc-119(ed3) III; ltIs38 [pAA1; pie-1::GFP::PH(PLC1delta1); unc-119 (+)]*
OD70	mCherry::PH	*unc-119(ed3) III; ltIs44[pAA173; pie-1::mCherry::PH(PLC1delta1); unc-119 (+)] V.*
OD120	GFP::ANI-1(ΔNT)	*unc-119(ed3) III; ltIs58 [pASM16; pie-1/GFP-TEV-Stag::ANI-1(aa171-1205); unc-119 (+)]*
OD124	GFP::ANI-1(ΔCT)	*unc-119(ed3) III; ltIs60 [pASM15; pie-1/GFP-TEV-Stag::ANI-1(aa2-754); unc-119 (+)] obligate het.*
SA245	mCherry::HIS	*unc-119(ed3); tjIs57 [pie-1::mCherry::his-48; unc-119(+)]*

Strain #	Marker(s)	Allele	Cross
MG390	NMY-2::GFP; GFP::HIS	-	JJ1473 x AZ212
MG508	mCherry::PH; GFP::ANI-1	-	OD70 x OD38
MG511	mCherry::PH; GFP::Tubulin	-	OD70 x AZ244
MG529	NMY-2::GFP; GFP::HIS	*zyg-9(b244)*	MG390 X DH244
MG535	GFP::PH; mCherry::HIS	-	OD58 x SA245
MG537	PIE-1::GFP; mCherry::HIS	-	JH1327 x SA245
MG541	GFP::PH	*zyg-9(b244)*	OD58 X DH244
MG542	GFP::ANI-1; mCherry::HIS	-	OD38 x SA245
MG543	GFP::PAR-2; mCherry::HIS	-	KK866 x SA245
MG559	GFP::PAR-2; mCherry::HIS	*mat-1(ax161)*	MG543 x DS77
MG561	GFP::ANI-1(ΔCT); mCherry:Tubulin	*mat-1(ax161)*	MG583 x DS77
MG562	GFP::ANI-1(ΔNT); mCherry::Tubulin	*mat-1(ax161)*	MG581 x DS77
MG580	GFP::ANI-1; mCherry::Tubulin	-	OD38 x JA1559
MG581	GFP::ANI-1(ΔNT); mCherry::Tubulin	-	OD120 x JA1559
MG583	GFP::ANI-1(ΔCT); mCherry::Tubulin	-	OD124 x JA1559